

# Surface Chemistry of CN Bond Formation from Carbon and Nitrogen Atoms on Pt(111)

Eldad Hecceg and Michael Trenary\*

Department of Chemistry, University of Illinois at Chicago, 845 West Taylor Street, Chicago, Illinois 60607-7061

Received: May 10, 2005; In Final Form: July 26, 2005

The mechanism of CN bond formation from CH<sub>3</sub> and NH<sub>3</sub> fragments adsorbed on Pt(111) was investigated with reflection absorption infrared spectroscopy (RAIRS), temperature-programmed desorption (TPD), and X-ray photoelectron spectroscopy (XPS). The surface chemistry of carbon–nitrogen coupling is of fundamental importance to catalytic processes such as the industrial-scale synthesis of HCN from CH<sub>4</sub> and NH<sub>3</sub> over Pt. Since neither CH<sub>4</sub> nor NH<sub>3</sub> thermally dissociate on Pt(111) under ultrahigh vacuum (UHV) conditions, the relevant surface intermediates were generated through the thermal decomposition of CH<sub>3</sub>I and the electron-induced dissociation of NH<sub>3</sub>. The presence of surface CN is detected with TPD through HCN desorption as well as with RAIRS through the appearance of the vibrational features characteristic of the aminocarbyne (CNH<sub>2</sub>) species, which is formed upon hydrogenation of surface CN at 300 K. The RAIRS results show that HCN desorption at ~500 K is kinetically limited by the formation of the CN bond at this temperature. High coverages of C<sub>ads</sub> suppress CN formation, but the results are not influenced by the coadsorbed I atoms. Cyanide formation is also observed from the reaction of adsorbed N atoms and carbon produced from the dissociation of ethylene.

## Introduction

The C–N coupling reaction to form CN on the Pt(111) surface is directly relevant to the use of platinum gauze catalysts in the industrial synthesis from CH<sub>4</sub> and NH<sub>3</sub> of hydrogen cyanide, an important chemical intermediate for products such as nylon.<sup>1</sup> In the absence of oxygen (Degussa process), the catalytic reaction is strongly endothermic and the heat must be supplied (~1500 K) externally by burning fuel, typically more CH<sub>4</sub> in another chamber. In contrast, addition of oxygen (Andrussow process) gives a net exothermic reaction. This later process has been used industrially to synthesize HCN since the 1940s.<sup>2</sup> In this paper we focus on the system without the presence of coadsorbed oxygen.

The synthesis of HCN over polycrystalline platinum has been the subject of several laboratory-scale studies at both atmospheric and reduced pressure.<sup>3–6</sup> Given that several competing reactions, such as NH<sub>3</sub> decomposition to N<sub>2</sub> and H<sub>2</sub>, would seem to be favored by equilibrium thermodynamics, it is surprising that the reaction can occur at all, particularly at total pressures as low as 1 Torr. The kinetics of HCN formation in both the absence<sup>4,5</sup> and the presence<sup>6</sup> of O<sub>2</sub> was studied in detail by Hasenberg and Schmidt. They reached several important conclusions. First, the reaction is definitely metal catalyzed, as opposed to occurring in the gas phase from reactive intermediates produced by the heated surface. Second, the rate law indicates a simple Langmuir–Hinshelwood mechanism, which implies that the key steps in the reaction occur between adsorbed species and therefore can be mimicked in UHV studies. Third, the coverage of surface carbon must be high enough to suppress NH<sub>3</sub> decomposition to N<sub>2</sub> and H<sub>2</sub> but not so high as to poison the surface. Fourth, the same basic mechanism applies to the reaction over both Pt and Rh. In one model reactor study they provide indirect evidence for the formation of CN through the

coupling reaction of surface C and N atoms.<sup>5</sup> The surface CN is then hydrogenated to HCN. However, in another study they speculate that surface CH<sub>z</sub> and NH<sub>y</sub> may be involved in a surface reaction to form a CNH<sub>z</sub> species ( $z \geq 2$ ), which is then dehydrogenated to HCN.<sup>4</sup> Therefore, to definitely establish the key reaction steps in catalytic HCN synthesis, identification of the surface species that combine to form the C–N bond is of great importance.

Secondary ion mass spectrometry (SIMS) has been used to detect C–N coupling reactions on Rh(111)<sup>7</sup> and Rh-loaded CeO<sub>x</sub>(111).<sup>8</sup> However, to our knowledge, there are no previous reports of this reaction on a platinum surface. The fact that the actual catalyst for HCN synthesis is a 90% Pt–10% Rh gauze makes a study on a platinum surface more relevant to the catalytic reaction. Since Pt has a relatively high ionization potential, which significantly lowers the probability of secondary ion formation, static SIMS is not a good choice for observing surface processes on Pt(111). In addition, the detection efficiency is substantially lower for relatively high mass clusters in the case of Pt compared to secondary ions that come from the first- or second-row transition metals. Finally, SIMS is a destructive technique that is difficult to quantify. Therefore, in this study we use TPD of HCN ( $m/e = 27$ ) as a means to detect CN bond formation. In the absence of hydrogen, CN desorbs as cyanogen (C<sub>2</sub>N<sub>2</sub>) in the range of 600–800 K,<sup>9</sup> but cyanogen desorption was not detected here. Surface CN can also be sensitively detected through its hydrogenation to the aminocarbyne species (CNH<sub>2</sub>), which has a strong and characteristic RAIR spectrum.<sup>10,11</sup> If CN bond formation occurs below ~350 K (the onset of H<sub>2</sub> desorption) and there is hydrogen on the surface, then we should expect to see the CNH<sub>2</sub> spectrum. If however the formation temperature is above 350 K, annealing a mixed CH<sub>x</sub>/NH<sub>y</sub> overlayer to various temperatures, cooling to 300 K, and then exposing to H<sub>2</sub> will permit the detection of any CN on the surface through the appearance of the CNH<sub>2</sub> spectrum.

\* Corresponding author. E-mail: mtrenary@uic.edu.

Both  $\text{CH}_4$  and  $\text{NH}_3$  have very small dissociative sticking probabilities on Pt(111).<sup>12–14</sup> Therefore, the reactive surface species that form during catalytic processes involving  $\text{CH}_4$  and  $\text{NH}_3$  must be generated by other means. Methyl iodide ( $\text{CH}_3\text{I}$ ) provides a convenient means to generate surface  $\text{CH}_x$  ( $x = 0–3$ ) species. The weak C–I bond dissociates below 200 K to yield surface methyl ( $\text{CH}_3$ ) groups, which then further decompose stepwise to finally give surface C atoms.<sup>15,16</sup> The coadsorbed iodine does not strongly influence the surface chemistry of hydrocarbons except for a site-blocking effect at higher coverages, as shown by comparing  $\text{CH}_3$  on Pt(111) deposited from the gas phase with  $\text{CH}_3$  produced from the dissociation of  $\text{CH}_3\text{I}$ .<sup>17,18</sup> Similarly, we find that the presence of coadsorbed iodine has minimal influence on the C–N coupling reaction.

Ammonia does not dissociate on Pt(111) at low pressures and temperatures. It desorbs molecularly in two stages: a lower binding energy state  $\beta$  (second layer) that is populated at higher coverages and desorbs at 120–180 K and an  $\alpha$  state representing molecules directly bonded to the platinum surface and desorbing over the range of 200–450 K.<sup>13,14</sup> However, it has been reported that  $\text{NH}_3$  can decompose on Pt surfaces under conditions other than UHV and low temperature. Vajo and co-workers<sup>19</sup> found ready decomposition under a steady flux at a pressure of  $\sim 1 \times 10^{-6}$  Torr and temperatures of 300–600 K. On the other hand, adsorbed  $\text{NH}_3$  on Pt(111) is readily dissociated through electron irradiation to form N, NH, and  $\text{NH}_2$  species on the surface.<sup>20</sup> Our present apparatus is arranged such that with the sample in the IR position it can be exposed to an electron beam from our LEED optics, which can be defocused to cover a large area. In this way we were able to induce  $\text{NH}_3$  decomposition and generate surface  $\text{NH}_y$  ( $y = 0–2$ ) species and study the reaction of these species with  $\text{CH}_x$  ( $x = 0–3$ ) to form CN. We reported our basic observation of C–N coupling in this system in a brief earlier publication.<sup>21</sup> Here we provide additional details and insights into the reaction.

## Experimental Section

The results were obtained in two separate UHV chambers. The XPS results were obtained in a chamber (chamber 1) with a base pressure of  $\sim 2 \times 10^{-10}$  Torr. The system has been described in detail elsewhere.<sup>22</sup> In brief, the UHV chamber is equipped with low-energy electron diffraction (LEED), an X-ray photoelectron spectroscopy (XPS) system, a quadrupole mass spectrometer (QMS) for TPD, and a Fourier transform infrared (FTIR) spectrometer for RAIRS studies. The XPS system consists of a VG CLAM2 hemispherical analyzer and X-ray source. Mg  $K\alpha$  radiation was used for the XPS study, and the spectrometer was calibrated with the Pt  $4f_{7/2}$  peak at a binding energy of 71.2 eV. All TPD and RAIRS experiments were performed in a second chamber (chamber 2) with a base pressure of  $\sim 1 \times 10^{-10}$  Torr. A detailed description of this system can be found elsewhere.<sup>23</sup> In brief, it consists of a stainless steel UHV chamber equipped for Auger electron spectroscopy (AES), LEED, and TPD experiments with a QMS. It is also coupled to a commercial FTIR spectrometer (Bruker IFS 66v/S). The IR beam enters and exits the UHV chamber through differentially pumped O-ring sealed KBr windows and passes through a polarizer before reaching an IR detector. To achieve maximum sensitivity in the NH and CH stretch regions, all RAIR spectra reported here were obtained with a liquid nitrogen cooled InSb detector with a low wavenumber cutoff near  $1950 \text{ cm}^{-1}$  and a tungsten IR source. In cases where the sample was annealed to a temperature above 85 K, the sample was then cooled back to 85 K before the IR spectrum was acquired. The background

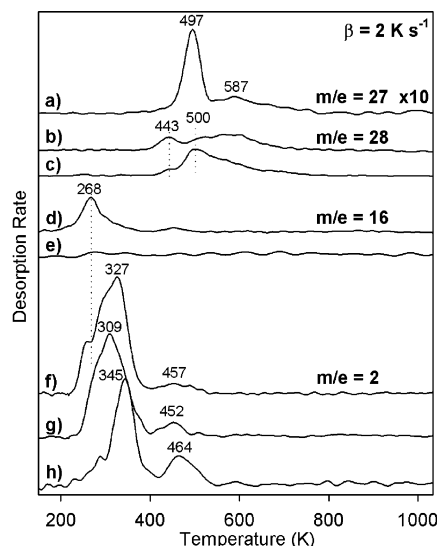


**Figure 1.** (a, b, d, and f) TPD spectra for  $m/e = 27$  (HCN), 28 ( $\text{N}_2/\text{CO}$ ), 16 ( $\text{CH}_4$ ), and 2 ( $\text{H}_2$ ), respectively, obtained after exposing Pt(111) to 0.2 L of  $\text{CH}_3\text{I}$  and 0.2 L of  $\text{NH}_3$  at 85 K followed by 100 eV  $e^-$  beam bombardment. (c and g) TPD spectra for  $m/e = 28$  ( $\text{N}_2/\text{CO}$ ) and 2 ( $\text{H}_2$ ) obtained after 0.2 L of  $\text{NH}_3$  has been  $e^-$  beam irradiated at 85 K. (e and h) TPD spectra for  $m/e = 16$  ( $\text{CH}_4$ ) and 2 ( $\text{H}_2$ ) obtained after 0.2 L of  $\text{CH}_3\text{I}$  has been  $e^-$  beam irradiated at 85 K.

reference spectrum was also taken at 85 K. A series of TPD experiments have been performed to correlate the exposures and establish the reproducibility between the two chambers and establish if the same surface conditions prevailed during the TPD, RAIRS, and XPS experiments. The Pt(111) surface was cleaned and judged free of impurities by a standard procedure described earlier.<sup>10</sup> The methyl iodide ( $\text{CH}_3\text{I}$ ) was purchased from Alfa Aesar Co. with a quoted purity of 99.5% and further purified by transferring it to a glass bulb and subjecting it to five freeze–pump–thaw cycles using a liquid nitrogen bath. It was then placed in a dry-ice–acetone bath and condensed into another glass bulb cooled by liquid nitrogen. Finally, it was shielded from the light because of its tendency to photolyze.  $\text{NH}_3$ ,  $\text{H}_2$ , and  $\text{C}_2\text{H}_4$  were purchased from Matheson Tri-Gas Inc. with quoted purities of 99.9992%, 99.9999%, and 99.99%, respectively, and used without further purification. A series of TPD experiments have been performed to correlate exposures with absolute coverages. Exposures of  $\sim 0.2$ , 2.5, and 2.0 L are necessary to saturate the first layer of  $\text{NH}_3$ ,  $\text{CH}_3\text{I}$ , and  $\text{C}_2\text{H}_4$ , respectively. These coverages are correlated with the absolute coverages by comparison with data available in the literature.<sup>14,15,24</sup> We used electron exposures of  $\sim 2 \times 10^{15}$  electrons per  $\text{cm}^2$  in all experiments reported here.

## Results

**(1) Detection of CN Bond Formation.** (i) *Temperature-Programmed Desorption.* Figure 1 shows TPD traces of the most relevant desorption products in the course of CN bond formation on Pt(111) from  $\text{CH}_3$  and  $\text{NH}_3$  fragments. The fact that the CN group can be formed under UHV on Pt(111) is demonstrated by the observation of HCN desorption in Figure 1a. After exposing the surface to 0.2 L of  $\text{CH}_3\text{I}$  and 0.2 L of  $\text{NH}_3$  at 85 K followed by bombardment by 100 eV electrons, HCN ( $m/e = 27$ ) is observed at 497 K with a high-temperature shoulder at 587 K. Following the direct adsorption of HCN on Pt(111), HCN desorbs at a lower temperature of  $\sim 460$  K.<sup>21,25</sup> Various control experiments were performed that proved that the HCN

is produced only when  $\text{NH}_3$ ,  $\text{CH}_3\text{I}$ , and electron irradiation are used.<sup>21</sup>

For the same conditions that lead to desorption of HCN (Figure 1a), Figure 1 also shows results for  $\text{CO}/\text{N}_2$  ( $m/e = 28$ ) (Figure 1b),  $\text{CH}_4$  ( $m/e = 16$ ) (Figure 1d), and  $\text{H}_2$  ( $m/e = 2$ ) (Figure 1f). These results are compared with the cases of irradiation with 100 eV electrons of surfaces on which only  $\text{NH}_3$  (Figure 1c and 1g) or only  $\text{CH}_3\text{I}$  (Figure 1e and 1h) is adsorbed. Although in principle the  $m/e = 28$  signals in Figure 1c and 1b could be due to either desorption of  $\text{N}_2$  or  $\text{CO}$  adsorbed from the background, we established that the peaks at 443 K in b and c are due to  $\text{CO}$  with the higher temperature features due to  $\text{N}_2$ . This is based on the fact that  $\text{CO}$  is known to desorb from the clean surface at  $\sim 440$  K<sup>26</sup> and by comparison of the  $m/e = 28$  traces in Figure 1b and 1c with the  $m/e = 12$  and 14 signals (not shown), which are predominantly due to  $\text{CO}$  and  $\text{N}_2$ , respectively. The decrease in the  $\text{N}_2$  desorption at  $\sim 500$  K in Figure 1b ( $\text{CH}_3\text{I} + \text{NH}_3 + e^-$ ) compared to Figure 1c ( $\text{NH}_3 + e^-$ ) is likely due to consumption of surface N atoms by the CN bond formation reaction.

Desorption of  $\text{H}_2$  corresponding to the conditions for HCN formation in Figure 1a is shown in Figure 1f. The  $\text{H}_2$  peak observed at 457 K is attributed to the decomposition of surface NH and/or CH and is seen at essentially the same temperature of 452 K for electron irradiation of  $\text{NH}_3$  adsorbed alone (Figure 1g) and at 464 K for electron irradiation of  $\text{CH}_3\text{I}$  alone (Figure 1h). The lower temperature  $\text{H}_2$  desorption peaks in Figure 1f, 1g, and 1h correspond to  $\text{H}_2$  recombinative desorption from hydrogen adsorbed from the background and from hydrogen produced through the dehydrogenation of  $\text{NH}_3$  and  $\text{CH}_3$ .<sup>27,28</sup> The lower amount of  $\text{H}_2$  desorption at 457 K in Figure 1f compared with the peaks at 452 and 464 K in Figure 1g and 1h is attributed to loss of hydrogen through HCN desorption.

Methane ( $m/e = 16$ ) desorption is not observed (Figure 1e) following a 0.2 L  $\text{CH}_3\text{I}$  exposure at 85 K and electron irradiation unless  $\text{NH}_3$  is present (Figure 1d). Comparison with the thermal decomposition<sup>15,29</sup> of  $\text{CH}_3\text{I}$  shows that exposure to the electron beam does not exert a strong influence on the surface chemistry of this molecule. It therefore follows that electron irradiation is needed only to induce  $\text{NH}_3$  dissociation. This is confirmed by a series of TPD experiments (not shown here) that show little or no difference in the  $m/e = 27$  trace when both  $\text{NH}_3$  and  $\text{CH}_3\text{I}$  are  $e^-$  irradiated compared to when only  $\text{NH}_3$  is irradiated and then  $\text{CH}_3\text{I}$  adsorbed afterward. At the low initial  $\text{CH}_3\text{I}$  coverages corresponding to the 0.2 L exposures used in Figure 1, dehydrogenation dominates the thermal chemistry when  $\text{CH}_3\text{I}$  is adsorbed alone and no  $\text{CH}_4$  desorption is observed, which is in agreement with previous studies.<sup>29</sup> However, the electron-induced dissociation makes additional hydrogen available, so that hydrogenation of the  $\text{CH}_3$  groups formed from the low-temperature breaking of the C–I bond of  $\text{CH}_3\text{I}$  can compete with the  $\text{CH}_3$  dehydrogenation reaction, and methane desorption is observed. This interpretation is supported by the presence of a small valley at 268 K in the  $\text{H}_2$  desorption shown in Figure 1f.

(ii) *Reflection Absorption Infrared Spectroscopy.* The use of RAIRS to detect the C–N coupling reaction is demonstrated in Figure 2. After exposing the Pt(111) surface to 0.2 L of  $\text{CH}_3\text{I}$  and 0.2 L  $\text{NH}_3$  at 85 K, it was irradiated with 100 eV electrons and annealed to 450, 500, and 550 K. After each anneal the sample was cooled to 300 K, exposed to 10 L of  $\text{H}_2$ , and then cooled to 85 K, where the spectra were acquired.

As previous work has shown,<sup>10,11</sup> if there is CN on the Pt(111) surface, then  $\text{H}_2$  exposure at 300 K should produce  $\text{CNH}_2$

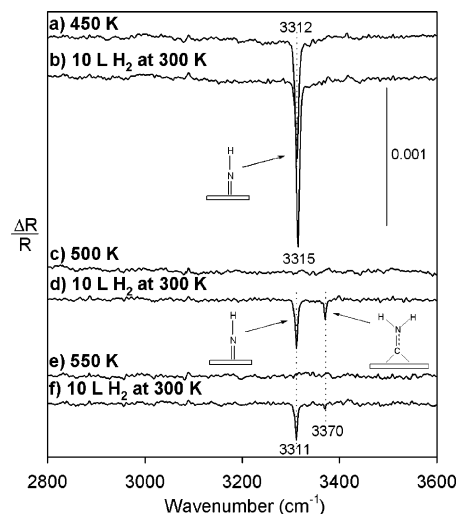


**Figure 2.** RAIR spectra obtained after exposing 0.2 L of  $\text{CH}_3\text{I}$  and 0.2 L of  $\text{NH}_3$  to the sample at 85 K followed by  $e^-$  beam irradiation with subsequent heating to the indicated temperatures and exposure to 10 L of  $\text{H}_2$  at 300 K.

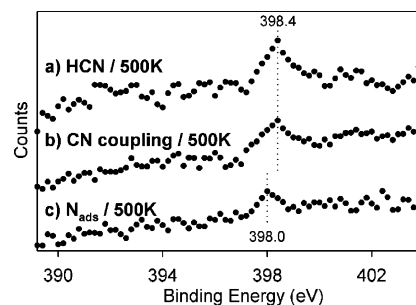


**Figure 3.** N 1s XPS peak obtained after (a) exposing 2.0 L of HCN to the sample at 85 K, followed by annealing to 500 K, (b) annealing to 500 K a surface that had been exposed to 0.2 L of  $\text{CH}_3\text{I}$ , 0.2 L of  $\text{NH}_3$ , and 100 eV electrons at 85 K, and (c) annealing to 500 K a surface that had been exposed to 0.2 L of  $\text{NH}_3$  and 100 eV electrons at 85 K.

with an NH symmetric stretch in the range of 3365–3370  $\text{cm}^{-1}$ . The 450 K anneal yields an intense peak at 3312  $\text{cm}^{-1}$ , which grows in intensity and shifts to 3315  $\text{cm}^{-1}$  after  $\text{H}_2$  exposure. This peak is due to the NH species, and we described its properties in detail elsewhere.<sup>27</sup> There is no peak due to  $\text{CNH}_2$  for the 450 K anneal nor for any annealing temperatures below 450 K. The 500 K anneal eliminates the  $\nu(\text{NH})$  peak of the NH species, which reappears at 3311  $\text{cm}^{-1}$  after  $\text{H}_2$  exposure due to rehydrogenation of surface N atoms. In addition,  $\nu(\text{NH})$  of the  $\text{CNH}_2$  species now appears at 3370  $\text{cm}^{-1}$ , demonstrating that the 500 K anneal leads to formation of CN on the surface. This peak is still present after a 550 K anneal but has a lower intensity.

(iii) *X-ray Photoelectron Spectroscopy.* In Figure 3 we compare XPS N 1s binding energies for CN produced by HCN dissociation (Figure 3a) with CN produced by the C–N coupling reaction (Figure 3b). In both cases peaks are centered at 398.4 eV, a N 1s binding energy that is characteristic of the CN group.<sup>30</sup> Figure 3c is a control experiment showing the N 1s binding energy of N atoms adsorbed on Pt(111). The N-covered surface was produced by a 0.2 L  $\text{NH}_3$  exposure at 85 K, irradiation with 100 eV electrons to dissociate the ammonia, and annealing to 500 K to dissociate any ammonia dissociation fragments and desorb hydrogen. The surface was then cooled back to 85 K, where the spectrum was obtained. The results provide further proof of the formation of CN from the surface  $\text{C}_1$  and  $\text{N}_1$  species present. Although the signal-to-noise ratio is

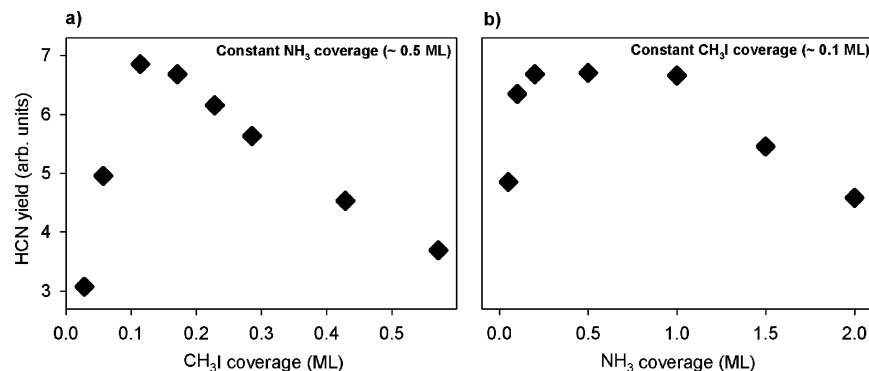


**Figure 4.** (a) HCN yield as a function of CH<sub>3</sub>I coverage for a fixed initial NH<sub>3</sub> coverage of  $\sim 0.5$  ML. (b) HCN yield as a function of NH<sub>3</sub> coverage for a fixed initial CH<sub>3</sub>I coverage of  $\sim 0.1$  ML. The HCN yield is equal to the area below the TPD curve for  $m/e = 27$ .

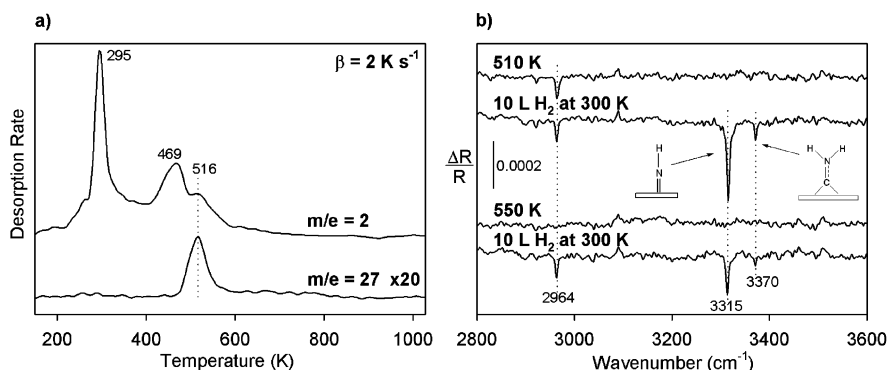


**Figure 5.** (a) TPD spectra for  $m/e = 2$  (H<sub>2</sub>) and 27 (HCN) obtained after exposing Pt(111) to 0.1 L of C<sub>2</sub>H<sub>4</sub> and 0.2 L of NH<sub>3</sub> at 85 K followed by 100 eV e<sup>-</sup> beam bombardment. (b) RAIRS spectra obtained after exposing 0.1 L of C<sub>2</sub>H<sub>4</sub> and 0.2 L of NH<sub>3</sub> to the sample at 85 K followed by e<sup>-</sup> beam irradiation with subsequent heating to the indicated temperatures and exposure to 10 L of H<sub>2</sub> at 300 K.

low, comparison of the N 1s shape in the three spectra suggests a shoulder on the low binding energy side of the peak in Figure 3b, consistent with the presence of both CN molecules and N atoms, as indicated by the RAIRS results.

**(2) Coverage Dependence. Temperature-Programmed Desorption.** Figure 4 shows the dependence of HCN yield from a series of TPD experiments where we varied the CH<sub>3</sub>I coverage for a fixed initial NH<sub>3</sub> coverage and vice versa. The HCN yield is defined as the area of the  $m/e = 27$  TPD peak. A monolayer (ML) is defined here as the saturated first layer of NH<sub>3</sub> ( $\alpha$ -NH<sub>3</sub>) or CH<sub>3</sub>I. By this definition, 1 ML of ammonia corresponds to one NH<sub>3</sub> molecule per four surface Pt atoms<sup>14</sup> while for methyl iodide it corresponds to one CH<sub>3</sub>I molecule per five surface atoms.<sup>15</sup>

The initial NH<sub>3</sub> coverage of approximately 0.5 ML was achieved by a 0.1 L exposure of NH<sub>3</sub> at 85 K. The surface was then bombarded with 100 eV electrons and exposed to different amounts of CH<sub>3</sub>I. The HCN yield reaches a maximum for 0.10–0.15 ML of CH<sub>3</sub>I, after which it drops significantly, implying that either CH<sub>3</sub>I itself or one of its dissociation products causes the quenching of the C–N coupling reaction. Figure 4b shows the HCN yield vs NH<sub>3</sub> coverage for a fixed initial CH<sub>3</sub>I coverage of  $\sim 0.1$  ML for an experiment in which 0.2 L of CH<sub>3</sub>I was exposed at 85 K followed by NH<sub>3</sub> exposure and e<sup>-</sup> beam irradiation. The HCN yield increases up to 0.2 ML of NH<sub>3</sub>, after which it remains essentially constant up to 1.0 ML. Up to 1.0 ML the HCN yield behavior is consistent with the reaction of all of the surface carbon by nitrogen with the plateau in HCN yield reached when all of the carbon has been consumed. The decrease in the amount of HCN for NH<sub>3</sub> coverages above 1 ML can be attributed to the build-up of second- ( $\beta$ -NH<sub>3</sub>) and higher order layers<sup>13,14</sup> of NH<sub>3</sub> that shield the  $\alpha$  state of NH<sub>3</sub> from the electrons, thus preventing dissociation.

**(3) C–N Coupling in the Absence of Iodine.** Although CH<sub>3</sub>I is a convenient source of C<sub>1</sub> hydrocarbons, it is desirable to verify the benign role of coadsorbed iodine by using a different source of carbon in the C–N coupling reaction. In a separate study of submonolayer coverages of C<sub>2</sub>H<sub>4</sub> on Pt(111), we have shown that C–C bond scission is feasible at temperatures above 450 K.<sup>31</sup> Therefore, surface carbon atoms can be produced from ethylene decomposition well below the CN bond formation temperature. After the surface was exposed to 0.1 L of C<sub>2</sub>H<sub>4</sub> and 0.2 L of NH<sub>3</sub> at 85 K and then exposed to the electron beam, HCN ( $m/e = 27$ ) is observed to desorb with a peak temperature of 516 K in Figure 5a, demonstrating that C–N coupling occurs under these circumstances. The fact that the HCN TPD peak in Figure 5a is 19 K above what was seen in Figure 1 when CH<sub>3</sub>I was used as the source of carbon atoms may be due to the HCN desorption being limited by C–C bond scission.

In addition to TPD, RAIRS also reveals the presence of the CN coupling reaction when ethylene is used as the carbon source. The spectra in Figure 5b were obtained after the surface was first exposed to 0.1 L of C<sub>2</sub>H<sub>4</sub> and 0.2 L of NH<sub>3</sub> at 85 K and then exposed to the electron beam. Annealing to 510 K yields only one peak at 2964 cm<sup>-1</sup>, which is assigned to  $\nu(\text{CH})$  of the CH species. Further details on the formation and properties of CH formed from C<sub>2</sub>H<sub>4</sub> can be found elsewhere.<sup>31</sup> Upon hydrogen exposure at 300 K two new peaks are observed with the same assignments as for Figure 2d. The 3370 cm<sup>-1</sup> peak of CNH<sub>2</sub> demonstrates that the CN bond is formed, although the amount appears to be less based on the lower peak intensity than that observed for CH<sub>3</sub>I, even though the overall carbon coverage was the same in the two cases. Figure 6 shows the HCN yield as a function of initial ethylene coverage for an initial ammonia coverage of 0.5 ML. A similar dependence of

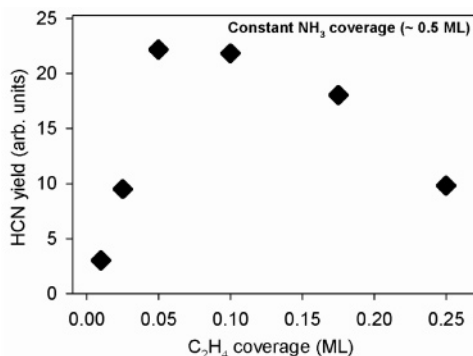


**Figure 6.** HCN yield from the integrated area of the  $m/e = 27$  TPD peak as a function of  $C_2H_4$  coverage for a fixed initial  $NH_3$  coverage of  $\sim 0.5$  ML. A ML of  $C_2H_4$  corresponds to one  $C_2H_4$  molecule per four Pt atoms.<sup>24</sup>

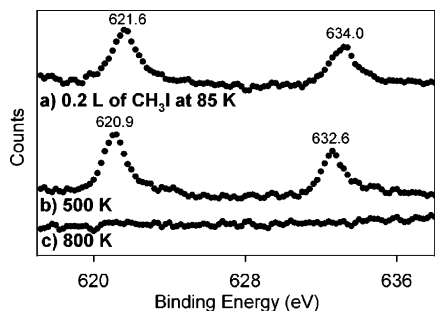


**Figure 7.** (a) I 3d XPS spectrum obtained after (a) exposing 0.2 L of  $CH_3I$  to the sample at 85 K, (b) annealing the sample in part a to 500 K, and (c) annealing the sample in part b to 800 K.

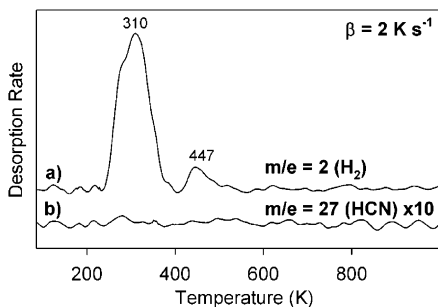


**Figure 8.** TPD results for  $m/e = 2$  ( $H_2$ ) (a) and 27 (HCN) (b) after the surface had been exposed to 0.2 L of  $CH_3I$  at 85 K, annealed to 800 K for 60 s, cooled to 85 K, exposed to 0.2 L of  $NH_3$ , and then exposed to 100 eV electrons.

HCN yield on  $C_2H_4$  coverage is observed as in Figure 4a, indicating that a low carbon coverage is most favorable for HCN production.

Another way to study the reaction in the absence of iodine is to perform the experiment after annealing the  $CH_3I$ -covered Pt(111) surface to 800 K for 60 s, which previous studies have suggested desorbs the iodine.<sup>15,16</sup> The XPS spectra of the I 3d region as a function of annealing temperature shown in Figure 7 verify this. The I  $3d_{5/2}$  and  $3d_{3/2}$  peaks at 621.6 and 634.0 eV, respectively, for 0.2 L of  $CH_3I$  adsorbed at 85 K shift to 620.9 and 632.6 eV but do not change intensity after a 500 K anneal, reflecting the fact that although the molecule dissociates at around 200 K, the iodine is still present at 500 K. These values in Figure 7b are typical of atomic iodine on surfaces.<sup>15,32</sup> However, the iodine peaks disappear completely after a 800 K anneal.

The TPD results in Figure 8 were obtained to determine if the carbon remaining on the surface after iodine desorption could

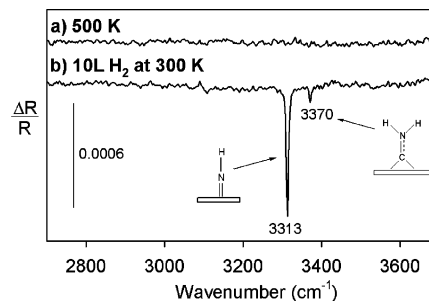


**Figure 9.** (a) RAIR spectrum acquired at 85 K after exposing the sample to 0.2 L of  $CH_3I$  at 85 K, annealing to 800 K for 60 s, cooling back to 85 K, exposing to 0.2 L of  $NH_3$ ,  $e^-$  beam irradiating, and annealing to 500 K. (b) RAIR spectrum acquired at 85 K after exposing 10 L of  $H_2$  at 300 K.

react with nitrogen to form cyanide. The surface was prepared by exposing to 0.2 L of  $CH_3I$ , annealing to 800 K, cooling to 85 K, exposing to 0.2 L of  $NH_3$ , followed by electron irradiation. The  $m/e = 2$  TPD trace in Figure 8a has a shape very similar to the one in Figure 1g. This is expected since annealing to 800 K decomposes all  $CH_3$  groups to surface C,<sup>15,16,29</sup> and in both Figures 8a and 1g hydrogen desorption is mainly due to the electron-induced decomposition of  $NH_3$ . However, no HCN desorption is observed (Figure 8b), indicating that surface CN, if present, is not detectable by this method. In contrast, the RAIRS data in Figure 9 do reveal that the C–N coupling reaction has taken place. The surface was prepared in the same way as for Figure 8. No peaks are present in the spectrum after the 500 K anneal. Upon exposure to 10 L of  $H_2$  at 300 K (Figure 9b), two peaks are observed with the same assignments as for Figure 2d. Although development of the  $CNH_2$  peak at 3370  $cm^{-1}$  confirms the presence of CN, the intensity of the peak is about one-half of that in Figure 2d. This is most likely due to conversion of some of the carbon into an unreactive graphitic form upon annealing to 800 K.<sup>15,33</sup>

## Discussion

According to model-reactor studies by Schmidt and Hickman,<sup>34</sup> the highly endothermic formation of HCN from  $CH_4$  and  $NH_3$  should not occur at all at temperatures below  $\sim 1000$  K. However, desorption of HCN at 497 K in Figure 1a is consistent with CN bond formation at or even below this temperature. We have shown earlier that the high-temperature shoulder at 587 K is not specific to the C–N coupling reaction but rather is related to HCN desorption from the step sites.<sup>21</sup> Moreover, RAIRS data in Figure 2e and 2f further confirm that there is no significant C–N coupling at temperatures above 500 K. This is probably due to the fact that above 500 K there are fewer N atoms available on the surface, as confirmed by the  $N_2$  desorption trace in Figure 1c. In addition, surface C atoms gain higher mobility, which could lead to formation of unreactive graphitic islands. The appearance of a  $CNH_2$  peak at 3370  $cm^{-1}$  in Figure 2d, after hydrogenation of the surface at 300 K following the 500 K anneal, reveals that CN bond formation likely coincides with the HCN desorption peak centered at 497 K (Figure 1a).

The appearance of the aminocarbene peak at 3370  $cm^{-1}$  in Figure 9b for the case when  $CH_3$  is completely dehydrogenated to C before the experiment was performed indicates that a hydrogenated form of carbon is not needed for the C–N coupling reaction to occur. The TPD results in Figure 1c and 1g showing  $N_2$  and  $H_2$  desorption peaks at 500 and 452 K, respectively, together with the disappearance of the NH stretch

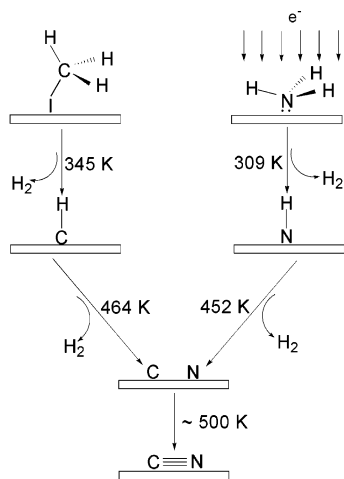


**Figure 10.** Proposed reaction mechanism of CN bond formation from  $\text{CH}_3\text{I}$  and  $\text{NH}_3$  on Pt(111).

peak at  $3315\text{ cm}^{-1}$  in the RAIR spectrum of Figure 2c after annealing to 500 K indicate that by 500 K only N atoms remain on the surface following electron-induced dissociation of  $\text{NH}_3$ . It therefore follows that the nitrogen-containing species in the C–N coupling reaction are adsorbed N atoms. These conclusions are summarized in Figure 10. Once formed at around 500 K, the surface CN can be hydrogenated to  $\text{CNH}_2$  if the surface is cooled to 300 K. The thermal dissociation of  $\text{CNH}_2$  occurs between 400 and 500 K and leads to desorption of HCN in the range of 450–600 K. Since dehydrogenation of the NH species is complete well before 500 K, the source of the hydrogen for the HCN desorption must originate from the dissociation products of  $\text{CH}_3\text{I}$ . We have direct RAIRS evidence<sup>31</sup> that the CH species is stable up to 500 K, and in Figure 1h the dissociation of CH gives rise to the  $\text{H}_2$  desorption peak at 464 K, which has a high-temperature tail that extends to about 550 K. Therefore, we conclude that the hydrogen in the HCN desorption observed in Figure 1 originates from the dissociation of CH.

From kinetic measurements of the gas-phase products in model reactor studies of the catalytic synthesis of HCN from  $\text{CH}_4$  and  $\text{NH}_3$  it was inferred that the reaction is feasible when the surface contains less than a monolayer of carbon and that it is strongly inhibited and even totally quenched by the presence of a carbon multilayer.<sup>5</sup> Our experiments provide more direct information on the influence of carbon coverage on HCN yield. At the simplest level we would expect the amount of CN formed on the surface to be limited by whichever is lower, the N coverage or the C coverage. If the initial coverage of  $\text{NH}_3$  is one molecule per eight surface atoms, then the amount of HCN formed should increase steadily up to a coverage of one molecule of  $\text{CH}_3\text{I}$  per eight Pt atoms. However, this is not the case, as shown in Figure 4a. Initially, the HCN yield increases, but then it suddenly drops after  $\sim 0.1$  ML of  $\text{CH}_3\text{I}$ . This coverage corresponds to 1 molecule of  $\text{CH}_3\text{I}$  for every 50 surface atoms, which is below what is implied by the reaction stoichiometry by a factor of  $\sim 6$ . At 500 K C and I atoms from  $\text{CH}_3\text{I}$  dissociation are present on the surface and, as already shown in Figure 9, the coupling reaction occurs even in the absence of  $\text{I}_{\text{ads}}$ . In other words, surface iodine is not directly involved in the coupling reaction, and therefore, it is highly unlikely that  $\text{I}_{\text{ads}}$  is the  $\text{CH}_3\text{I}$  dissociation product that is responsible for the quenching, especially in the low coverage regime (1  $\text{I}_{\text{ads}}$ /50 Pt atoms). Additional evidence can be found in Figure 6, where a molecule that does not contain iodine,  $\text{C}_2\text{H}_4$ , showed similar coverage dependence for HCN yield. Not surprisingly, the

coverage that completely poisons the reaction for  $\text{C}_2\text{H}_4$  is about one-half of that of  $\text{CH}_3\text{I}$ . This strongly suggests that surface carbon is responsible for deactivation of the surface, in agreement with the kinetic studies of Hasenberg and Schmidt.<sup>5</sup> They inferred that every C atom blocks three sites on their polycrystalline surface, and if we assume that this number is approximately the same for Pt(111), then the free sites on the surface necessary for C–N bond formation to occur could be completely blocked at higher carbon coverages. Furthermore, graphitic islands are much more easily formed at higher than lower carbon coverages. It then follows that at higher carbon coverages N atoms are able to react readily only with C atoms outside of ordered islands or at island edges, which would explain the inability to convert all of the carbon present on the surface to CN.

Comparison of Figures 4a and 6 shows that the maximum HCN yield is higher by a factor of  $\sim 3$  for ethylene than for  $\text{CH}_3\text{I}$ . However, RAIRS experiments (Figures 2d and 5b) show that the intensity of the aminocarbyne  $\nu(\text{NH})$  peak in the case of  $\text{C}_2\text{H}_4$  is actually smaller than that obtained from  $\text{CH}_3\text{I}$ , suggesting that less CN is formed from C and N atoms in the former case. This seemingly contradictory observation can be readily explained by the fact that more hydrogen is available at 500 K when  $\text{C}_2\text{H}_4$  is used as a source of C atoms. Previous studies<sup>35</sup> of ethylene decomposition on Pt(111) have shown that hydrogen desorption can be easily observed up to  $\sim 600$  K. This also can be seen in Figure 5a for the  $m/e = 2$  trace. In separate experiments of hydrogen desorption we determined that the amount of hydrogen evolving from the decomposition of  $\text{C}_2\text{H}_4$  at 500 K is much higher than that for the  $\text{CH}_3\text{I}$ . It follows then that most of the CN molecules formed from  $\text{C}_2\text{H}_4$  are immediately hydrogenated and desorb as HCN. However, in the case of  $\text{CH}_3\text{I}$ , even if more C–N bonds are formed, not all of the CN formed can be hydrogenated because of the lack of hydrogen atoms on the surface.

Finally, there are various ways to extract kinetic parameters from thermal desorption data, provided certain assumptions are valid. Hagans et al.<sup>36</sup> reported HCN TPD results on Pt(111) and found that the HCN desorbs with a constant peak temperature at  $\sim 460$  K as a function of HCN exposure. They labeled the desorption at this temperature as the  $\beta$  state and attributed it to recombination of  $\text{H}_{\text{ad}}$  and  $\text{CN}_{\text{ads}}$ . Although recombinative desorption should lead to second-order kinetics, desorption at a constant peak temperature is a clear indication of first-order kinetics. We also observed HCN desorption at a constant temperature in the range of 460–500 K as a function of increasing HCN exposure to the clean Pt(111) surface and at various  $\text{CH}_3\text{I}$  and  $\text{NH}_3$  exposures in the case of the C–N coupling reaction. If the rate of the  $\beta$  HCN desorption is determined by the rate of aminocarbyne decomposition, then first-order desorption kinetics would be expected. Since RAIRS observations of the stability of aminocarbyne show that it decomposes in the temperature range of 400–500 K, it is reasonable to assume that aminocarbyne decomposition is rate determining for HCN desorption in this temperature range.

For first-order desorption with a peak temperature of 470 K and an assumed preexponential factor of  $10^{13}\text{ s}^{-1}$ , the Redhead equation<sup>37</sup> gives an activation energy of 128 kJ/mol, whereas assumed preexponentials of  $10^{15}$  and  $10^{11}\text{ s}^{-1}$  yield activation energies of 146 and 109 kJ/mol, respectively. A method described by Chan, Aris, and Weinberg (CAW)<sup>38</sup> permits both the preexponential and activation energy to be obtained from measurements of the peak temperature and peak width. By the CAW method we obtain a preexponential of  $5 \times 10^{13}\text{ s}^{-1}$  and

an activation energy of 128 kJ/mol. Since the HCN desorption that accompanies the C–N coupling reaction reported here occurs at a higher temperature than for HCN desorption following HCN exposure, it is reasonable to assume that the rate of HCN desorption here is limited by the rate of CN formation. With this assumption the rate constant for CN formation can be obtained. The CAW method applied to the HCN desorption peak at 497 K in Figure 1 yields a preexponential of  $8 \times 10^{10} \text{ s}^{-1}$  and an activation energy of 113 kJ/mol, whereas the Redhead equation with an assumed preexponential of  $10^{13} \text{ s}^{-1}$  yields an activation energy of 132 kJ/mol. A review<sup>39</sup> of the effect of lateral interactions on kinetic parameters extracted from TPD data notes that both the Redhead and CAW methods, although simple and easy to use, are invalid in the presence of lateral interactions except in the limit of zero coverage. For HCN desorption from Pt(111), the invariance of the peak position with coverage suggests that lateral interactions are small. The kinetic parameters obtained here from TPD data can be compared with the preexponential of  $10^{11 \pm 1} \text{ s}^{-1}$  and activation energy of  $210 \pm 15 \text{ kJ/mol}$  for the C–N coupling reaction on Rh(111) obtained from temperature-programmed SIMS data.<sup>7</sup> The higher activation energy is associated with the higher HCN desorption temperature of  $\sim 600 \text{ K}$  on Rh(111).

### Summary

We have demonstrated that the carbon–nitrogen coupling reaction that underlies the catalytic synthesis of HCN from ammonia and methane over platinum can be induced on the Pt(111) surface under UHV conditions. The experiments show that the carbon-containing and nitrogen-containing species involved in the coupling reaction are individual C and N atoms rather than hydrogen-containing  $\text{CH}_x$  or  $\text{NH}_y$  species. The formation of the CN species was detected both by desorption of HCN and by observation of the aminocarbyne species,  $\text{CNH}_2$ , with RAIRS following hydrogen exposure. The experiments further show that C–N bond formation occurs at  $\sim 500 \text{ K}$ . Electron-induced dissociation of ammonia was used to produce surface N atoms, whereas both  $\text{CH}_3\text{I}$  and  $\text{C}_2\text{H}_4$  were used to produce surface C atoms. Formation of surface CN is strongly dependent on carbon coverage, in agreement with previous kinetic studies.

**Acknowledgment.** We gratefully acknowledge support by a grant from the National Science Foundation (CHE-0135561).

### References and Notes

- (1) Satterfield, C. N. In *Heterogeneous Catalysis in Practice*; McGraw-Hill: New York, 1980.
- (2) Satterfield, C. N. In *Heterogeneous Catalysis in Industrial Practice*, 2nd ed.; McGraw-Hill: New York, 1991.
- (3) Koberstein, E. *Ind. Eng. Chem. Process Des. Dev.* **1973**, *12*, 444–448. Suárez, M. P.; Löffler, D. G. *J. Catal.* **1986**, *97*, 240. Dietz, A. G., III; Schmidt, L. D. *Appl. Catal. A: Gen.* **2000**, *180*, 287. Bodke, A. S.; Olschki, D. A.; Schmidt, L. D. *Appl. Catal. A: Gen.* **2000**, *201*, 13.
- (4) Hasenberg, D.; Schmidt, L. D. *J. Catal.* **1985**, *91*, 116.
- (5) Hasenberg, D.; Schmidt, L. D. *J. Catal.* **1986**, *97*, 156.
- (6) Hasenberg, D.; Schmidt, L. D. *J. Catal.* **1987**, *104*, 441.
- (7) van Hardeveld, R. M.; Schmidt, A. J. G. W.; Niemantsverdriet, J. W. *Catal. Lett.* **1996**, *41*, 125. van Hardeveld, R. M.; van Santen, R. A.; Niemantsverdriet, J. W. *J. Phys. Chem. B* **1997**, *101*, 7901. van Hardeveld, R. M.; Borg, H. J.; Niemantsverdriet, J. W. *J. Mol. Catal. A: Chem.* **1998**, *131*, 199.
- (8) Mullins, D. R.; Zhang, K. *J. Phys. Chem. B* **2001**, *105*, 1374.
- (9) Hoffmann, W.; Bertel, E.; Netzer, F. P. *J. Catal.* **1979**, *60*, 316.
- (10) Jentz, D.; Celio, H.; Mills, P.; Trenary, M. *Surf. Sci.* **1995**, *341*, 1.
- (11) Jentz, D.; Mills, P.; Celio, H.; Trenary, M. *Surf. Sci.* **1996**, *368*, 354.
- (12) Ukraintsev, V. A.; Harrison, I. *Surf. Sci.* **1993**, *286*, L571. Meixner, D. L.; George, S. M. *Surf. Sci.* **1993**, *297*, 27. Alberas-Sloan, D. J.; White, J. M. *Surf. Sci.* **1996**, *365*, 212.
- (13) Sexton, B. A.; Mitchell, G. E. *Surf. Sci.* **1980**, *99*, 523.
- (14) Fisher, G. B. *Chem. Phys. Lett.* **1981**, *79*, 452.
- (15) Zaera, F.; Hoffmann, H. *J. Phys. Chem.* **1991**, *95*, 6297.
- (16) Henderson, M. A.; Mitchell, G. E.; White, J. M. *Surf. Sci. Lett.* **1987**, *184*, L325.
- (17) Fairbrother, D. H.; Peng, X. D.; Viswanathan, R.; Stair, P. C.; Fan, J.; Trenary, M. *Surf. Sci.* **1993**, *285*, L455.
- (18) Fan, J.; Trenary, M. *Langmuir* **1994**, *10*, 3649.
- (19) Vajo, J. J.; Tsai, W.; Weinberg, W. H. *J. Phys. Chem.* **1986**, *90*, 6531.
- (20) Burns, A. R.; Stechel, E. B.; Jennison, D. R.; Li, Y. S. *J. Chem. Phys.* **1994**, *101*, 6318. Sun, Y.-M.; Sloan, D.; Ihm, H.; White, J. M. *J. Vac. Sci. Technol. A* **1996**, *14*, 1516. Bater, C.; Campbell, J. H.; Craig, J. H., Jr. *Surf. Interface Anal.* **1998**, *26*, 97.
- (21) Herceg, E.; Trenary, M. *J. Am. Chem. Soc.* **2003**, *125*, 15758.
- (22) Kang, D. H.; Trenary, M. *Surf. Sci.* **2000**, *470*, L13.
- (23) Brubaker, M. E.; Trenary, M. *J. Chem. Phys.* **1986**, *85*, 6100.
- (24) Mitchell, I. V.; Lennard, W. N.; Griffiths, K.; Massoumi, G. R.; Huppertz, J. W. *Surf. Sci.* **1991**, *256* (1–2), L598.
- (25) Celio, H.; Mills, P.; Jentz, D.; Pae, Y. I.; Trenary, M. *Langmuir* **1998**, *14*, 1379.
- (26) Norton, P. R.; Goodale, J. W.; Selkirk, E. B. *Surf. Sci.* **1979**, *83*, 189.
- (27) Herceg, E.; Mudiyansele, K.; Trenary, M. *J. Phys. Chem. B* **2005**, *109*, 2828.
- (28) Herceg, E.; Celio, H.; Trenary, M. *Rev. Sci. Instrum.* **2004**, *75* (8), 2545.
- (29) Henderson, M. A.; Mitchell, G. E.; White, J. M. *Surf. Sci.* **1991**, *248*, 279.
- (30) Sexton, B. A.; Hughes, A. E. *Surf. Sci.* **1984**, *140*, 227. Lindquist, J. M.; Ziegler, J. P.; Hemminger, J. C. *Surf. Sci.* **1989**, *210*, 27. Serafin, J. G.; Friend, C. M. *J. Phys. Chem.* **1988**, *92*, 6694.
- (31) Deng, R.; Herceg, E.; Trenary, M. *Surf. Sci.* **2004**, *573* (2), 310.
- (32) Zaera, F. *Surf. Sci.* **1989**, *219*, 453.
- (33) Land, T. A.; Michely, T.; Behm, R. J.; Hemminger, J. C.; Comsa, G. *J. Chem. Phys.* **1992**, *97* (9), 6774. Smirnov, M. Yu.; Gorodetskii, V. V.; Cholach, A. R.; Zemlyanov, D. Yu. *Surf. Sci.* **1994**, *311*, 308.
- (34) Schmidt, L. D.; Hickman, D. A. In *Catalysis of Organic Reactions*; Kosak, J. R., Johnson, T. A., Eds.; Marcel Dekker: New York, 1994; p 195.
- (35) Salmerón, M.; Somorjai, G. A. *J. Phys. Chem.* **1982**, *86*, 341.
- (36) Hagans, P. L.; Guo, X.; Chorkendorff, I.; Winkler, A.; Siddiqui, H.; Yates, J. T., Jr. *Surf. Sci.* **1988**, *203*, 1.
- (37) Redhead, P. A. *Vacuum* **1967**, *12*, 203.
- (38) Chan, C.-M.; Aris, R.; Weinberg, W. H. *Appl. Surf. Sci.* **1978**, *1*, 360.
- (39) Nieskens, D. L. S.; van Bavel, A. P.; Niemantsverdriet, J. W. *Surf. Sci.* **2003**, *546*, 159.